Applied Physics A (2023) 129:16
https://doi.org/10.1007/s00339-022-06297-z

Applied Physics A
Materials Science & Processing

S.I. : 50TH ANNIVERSARY OF APPLIED PHYSICS

Only gold can pull this off: mechanical exfoliations of transition metal dichalcogenides beyond scotch tape

Max Heyl[1] · **Emil J. W. List-Kratochvil**[1,2]

Received: 4 November 2022 / Accepted: 29 November 2022 / Published online: 9 December 2022

Abstract
Following in graphene's wake, the scotch tape method became the key enabler for the preparation of 2D materials, providing easy access to high-quality materials mainly limited by low yield. At this time, transition metal dichalcogenides (TMDC) received tremendous attention as a promising class of two-dimensional (2D) semiconductors. The motivation to reach the 2D limit of TMDCs and many other layered materials has long been set, and with the rise of gold-mediated exfoliations towards the millimeter scale, the stacking of these 2D single-layer building blocks into artificial 3D lattices is more relevant than ever. On this note, this review presents the recent developments in gold-mediated exfoliations beyond scotch tape, accompanied by a methods walkthrough for such a process. These matured gold exfoliations unlock a whole palette of 2D building blocks, ready for the assembly of macroscopic van der Waals heterostructures, or twistronics. Ultimately, mechanical exfoliation as a key enabler for high-quality single layers, evolved from scotch tape to gold, and became an even more potent tool in the process.

Keywords Transition metal dichalcogenides · Gold-mediated · Noble metal · Mechanical exfoliation · Template-stripped gold

1 Introduction

The isolation of graphene [1] as the first two-dimensional material boosted the interest in layered crystals as precursors to their single-layer forms [2]. But looking back in history, the first reported single layer was MoS_2, a transition metal dichalcogenide (TMDC), and pre-dates the isolation of graphene [1, 3]. In 1986 the idea to physically thin the layered structure of MoS_2 to a single layer has led to the first MoS_2 monolayers [3]. Here the basic idea relied on the separation of MoS_2 layers in the parent crystal via Li intercalation and subsequent reaction with H_2O, resulting in exfoliation via nascent H_2 separating the layers. Yet, the endeavor was purely curiosity driven and no application was shown, leaving the single-layer MoS_2 in a 2D winter for almost 20 years. In 2004 graphene entered the 2D game (for a historical survey see Fig. 1), this time thinned down to the single-layer limit via scotch tape [1]. Graphene reignited the interest in all single-layer materials due to its exotic physics accompanied by its two-dimensionality [1, 4–7]. As early as 2005 the first single-layer MoS_2 has been exfoliated with scotch tape and has been tested in a transistor [2]. Along these lines, transition metal dichalcogenides (TMDCs) received tremendous attention as a promising material class for two-dimensional semiconductors [8–17]. TMDCs are layered compounds where each three-atom thin layer consists of a sheet of transition-metal atoms (e.g., W, Mo) sandwiched by sheets of chalcogenide atoms (e.g., S, Se) [11, 16]. These three-atom thin sheets are stacked into their layered structures guided by weak van der Waals (vdW) interactions. Since the inter-layer interactions are weak, layers can be cleaved with ease, enabling the exfoliation of a single layer by means of physically thinning down the layered structure to the monolayer limit [2]. The efforts to reach the monolayer limit are easily motivated by a whole set of interesting attributes accompanying two-dimensional TMDCs [8, 9, 12, 13, 15–21]. The atomically flat nature allows effective manipulation via external stimuli, e.g.,

✉ Emil J. W. List-Kratochvil
emil.list-kratochvil@hu-berlin.de

[1] Institut für Physik, Institut für Chemie and IRIS Adlershof, Humboldt-Universität zu Berlin, Zum Großen Windkanal 2, 12489 Berlin, Germany

[2] Helmholtz-Zentrum Berlin für Materialien und Energie GmbH, Hahn-Meitner-Platz 1, 14109 Berlin, Germany

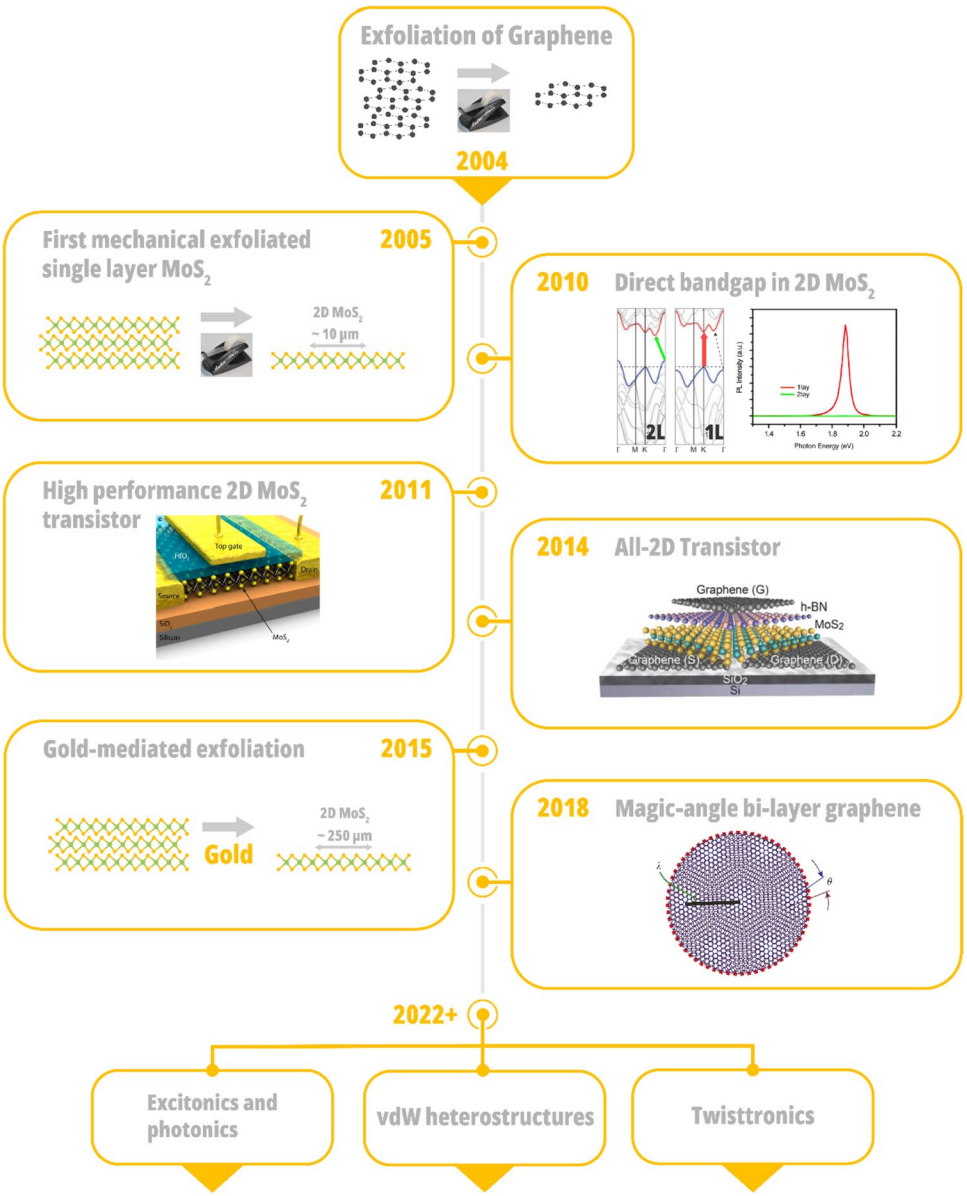

Fig. 1 Historical survey of 2D material research with a focus on TMDCs. Only a subset of important milestones is displayed. The mechanical exfoliation of graphene 2004 [1] reignited this research strand, closely followed by the first mechanical exfoliation of MoS_2 in 2005 [2]. The indirect-to-direct bandgap transition for MoS_2 demonstrated that 2D TMDCs unlock new physics in their single-layer limit (2010) [9, 21]. Soon high performing 2D MoS_2 transistors have been presented in 2011 [22], with all-2D transistors following in 2014 [31]. In 2015, gold was first used as the more capable successor of scotch tape to exfoliate large area single layers of TMDCs and more [32]. Lastly, the study on twisted bi-layer graphene's unconventional superconductivity boosted interest in twisted layered materials in 2018 [33, 34]. Overall, with large-scale exfoliations unlocked for high-quality 2D materials, there are several branches left to be further studied for beyond 2022. Figures adapted from several sources, citations and permissions given for each panel year: 2004, 2005: Adapted with permission from [35]. 2010: Left figure adapted with permission from [21]. Copyright 2010 American Chemical Society. Right figure is reprinted with permission from [9]. Copyright 2010 by the American Physical Society. 2011: Reprinted with permission from [36]. Copyright 2015 American Chemical Society. 2014: Reprinted with permission from [31]. Copyright 2014 American Chemical Society. 2018: Reprinted by permission from Springer Nature: Nature [34], copyright 2018

effective gating in the field-effect transistor (FET) [19, 22]. Furthermore, monolayer TMDCs exhibit indirect-to-direct band gap transitions [9, 21], high excitonic binding energies [12] and valley degrees of freedom in the electronic band structure [13]. The quest for high-quality and large-scale monolayer TMDCs fostered the development of different techniques [23, 24] ranging from bottom-up approaches like chemical vapor deposition (CVD) [11] to top-down routes via liquid or mechanical exfoliation [2, 11, 25, 26]. To date, all routes suffer from specific drawbacks, e.g., mechanical

exfoliation promises high-quality 2D materials, essentially limited by the 3D starting crystal quality, yet the process is limited regarding yield. Techniques like CVD are also very capable of producing high-quality 2D materials, but these usually require significantly more optimization for each 2D material composition as discussed in Sect. 3 [27, 28]. Overall, despite the limited yield, the versatility and ease of access of mechanical exfoliations made them a key enabler in the last years, where the high quality provided from the starting crystal especially shined in quantum transport studies in graphene and beyond [29, 30]. In this review, we will concentrate on mechanical exfoliation methods capable to isolate large-area and high-quality TMDC monolayers with high yield. We note that most of the TMDC studies have a clear focus on MoS_2, while the other TMDCs such as WS_2, $MoSe_2$ and WSe_2 are less frequently found. This does not reflect any disadvantages or diminished electronic properties of those latter compounds but is more related to the ready availability of high-quality MoS_2 parent crystals. This also has an impact on our review, where we often use MoS_2 as the prototypical TMDC. However, the exfoliations discussed here are not limited to TMDCs as discussed later.

Inspired by the pioneering work of Geim and Novoselov on tape-based mechanical exfoliation of graphene [1], tape-based exfoliation became the standard tool for 2D materials, also for TMDCs. However, it was apparent early on that the tape-based process is very limited in exfoliation yields, limiting its use beyond lab-scale experiments. To overcome these limitations scalable exfoliations beyond scotch tape have been investigated [37] and gold [32, 38–45], silver [46–48] as well as other noble metals [46, 48–50] have been identified to provide the needed adhesive forces via strong vdW [45] or "covalent-like quasi-bonding" (CLQB) [44] interactions with TMDCs to pull off a monolayer. Already early on it was noted that the yield and quality of the exfoliated monolayers are correlated with the availability of a smooth and clean metal surface [45]. This has led to a very promising route for mechanical exfoliation using the template-strip method [32, 42, 43] to provide ultra-flat and clean metal surfaces by freshly cleaving a gold film off an ultra-flat template substrate, accessing the smooth and uncontaminated former metal-template interface. In some studies, silver [47] was used for this template-strip method to yield large-area and high-coverage MoS_2 monolayers. The resulting methods rendered MoS_2 monolayer isolation with lateral dimensions up to millimeters [42–45, 47] a robust and accessible process, essentially limited by the dimensions of the precursor crystal interface. Additionally, these processes allow for the elegant implementation of a polymer-free transfer of exfoliated MoS_2 [43], mitigating the known issues of polymeric residues [51, 52]. Furthermore, to date, a whole zoo of 2D materials [53] exists, each material ready to be included as a 2D building block to utilize its properties in a new dimension. For instance, graphene has been employed as a 2D electrode [54], whereas hexagonal boron nitride (hBN) was employed as an encapsulation layer or dielectric, owing to its insulating behavior [55–57]. TMDCs promise new 2D semiconductor building blocks, enlarging the 2D toolbox, yet necessitating proper exfoliation and transfer to access the latter. Overall, mechanical exfoliation has served 2D materials research as a key enabler for these building blocks in high-quality and evolved from scotch tape towards gold to become a potent tool covering all aspects of TMDC-based research and beyond. In this review, metal-mediated exfoliations with a focus on gold are discussed. The overall focus of this review on TMDCs allows us to introduce some more properties of our prototypical TMDC, MoS_2, below.

2 Basic structural, electronic, and optical properties of MoS_2

Before going into medias res with respect to exfoliation and subsequent transfer processes, we give a brief introduction for the composition, structure, and electronic properties of 2D TMDCs as promising atomically flat direct band-gap semiconductors [11]. TMDCs are layered compounds (Fig. 2), where each three-atom thin layer consists of a sheet of transition-metal (TM) atoms (e.g., W, Mo) sandwiched by sheets of chalcogenide atoms (e.g., S, Se).

The chalcogen lone pairs terminate these layers, rendering the surface chemically stable and free of dangling bonds [11]. The sheets are stacked into layered structures guided by weak vdW interactions. Due to the pick & mix nature of TMDCs, several family members exist (about 40). In principle, there are metallic and semiconducting candidates, mainly depending on the d-orbital filling and coordination environment, i.e., crystal phase and transition metal group [11]. For instance, natural MoS_2 adopts the hexagonal 2H-phase (trigonal prismatic coordination, D3h point group), combined with the d-electron filling for a group 6 (Mo) transition metal, the Fermi Level (E_F) lies within the band gap, i.e., 2H-MoS_2 is semiconducting [11]. Besides the trigonal prismatic coordination mentioned above, there also exists octahedral coordination (D3d, 1T phase), which exhibits metallic behavior. The (thermodynamic) preference for one of these coordination modes is governed by the TMDC composition. Since the position of the Fermi Level is susceptible to d-electron filling, MoS_2 exfoliated via alkali metal intercalation (Li) is known to undergo a 2H-to-1T phase transition, related to the effective change in d-electron count via reduction [11, 20]. This further motivates the use of quality-preserving mechanical exfoliations. The semiconducting properties of 2H-MoS_2 are further detailed by inspecting the electronic band structure [21], as depicted in Fig. 3a.

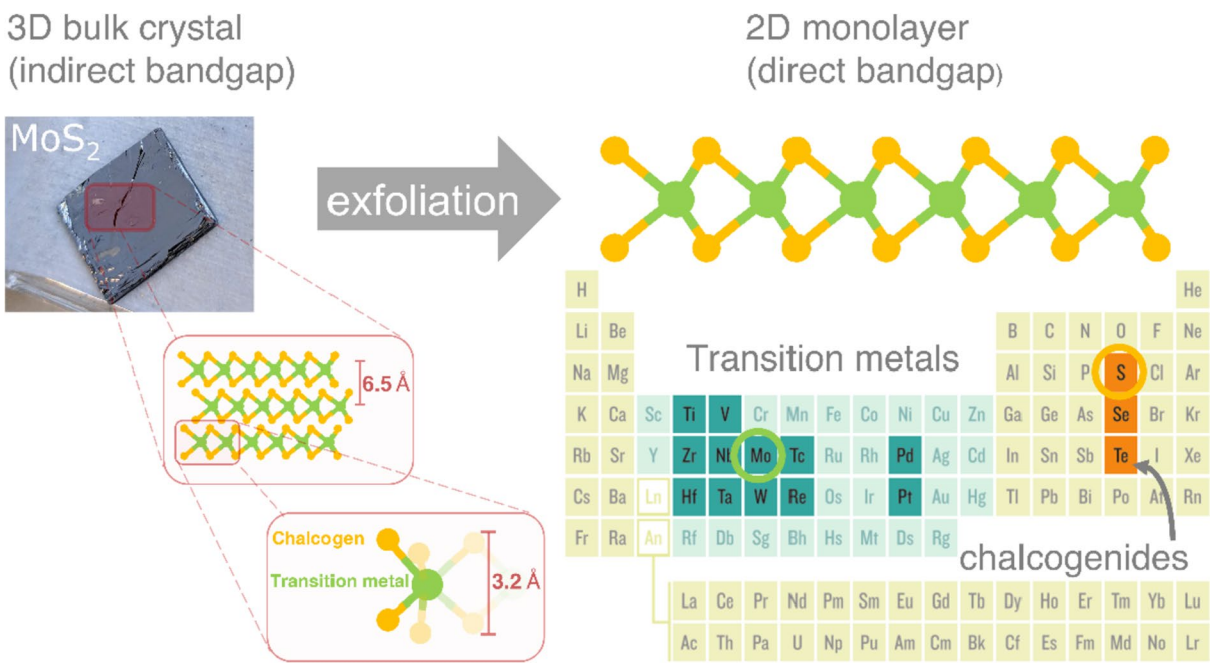

Fig. 2 Composition and structure of TMDCs [11, 17] showing the layered structures guided by weak vdW forces. Layers can be cleaved with ease, enabling mechanical exfoliation of single layers only three atoms thick. This exfoliation process is sketched by showing the transition from the bulk-layered crystal towards the single layer. It is important to note that these 2D materials, when compared to their 3D counterparts, can unlock new physics and properties directly related to their low-dimensional character, as seen in the direct bandgap for 2D MoS_2 [9, 21]. There are several TMDC combinations possible via pick & mix in the periodic table, as highlighted with green and orange colors for typical transition metals and chalcogenides, respectively. This opens a whole material library for TMDCs with different properties depending on the composition [11]. The most prominent candidate is MoS_2 and will often serve as a testbed for exfoliations. Adapted by permission from Springer Nature: Nature [58], copyright 2015

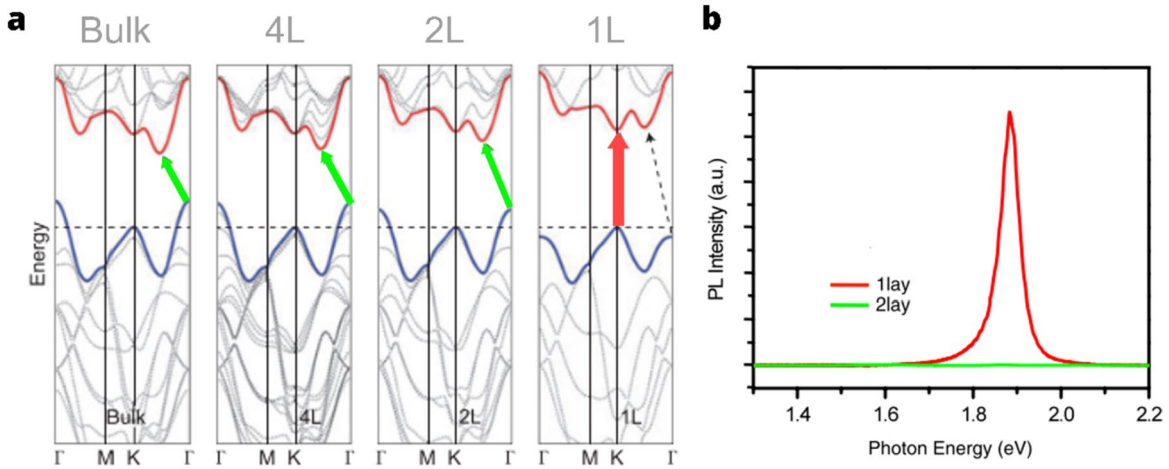

Fig. 3 Indirect-to-direct bandgap transition of 2D MoS_2. (a) Band structure for bulk, 4L, 2L and 1L MoS_2 [21]. The horizontal dashed line indicates the band maximum at the K point. The conduction and valence band edges are highlighted in red and blue, respectively. The lowest energy transition (bandgap) is only direct (vertical) for 1L MoS_2 [9, 21]. (b) PL spectra for 1L and 2L MoS_2 [9]. The bright emission from 1L MoS_2 is related to its direct bandgap, as compared to the bilayer (indirect bandgap). **a** Adapted with permission from [21]. Copyright 2010 American Chemical Society. **b** Reprinted with permission from [9]. Copyright 2010 by the American Physical Society

Bulk MoS_2 has an indirect band gap of circa 1.2 eV, [11] but once the 2D state is reached the band structure changes, enabling a direct band gap of 1.85 eV [11]. This allows for strong light emission as seen in the photoluminescence (PL)

spectra in Fig. 3b [9]. The bilayer only exhibits poor emission, as expected for an indirect band gap. The photophysics of 2D TMDCs are quite unique, with very pronounced excitonic behavior due to large excitonic binding energies in the order of several hundreds of meV [59]. Yet it is not in the scope of this work to detail these physics here, the reader is referred to an excellent review on this topic by Gang Wang et al. [12].

In principle, the surface of TMDCs is inert due to the lack of dangling bonds. However, real-world TMDCs contain a lot of defects [20, 60–63], e.g., sulfur vacancies (point defects). 2D materials essentially being only surface, defects have a high impact and depending on the preparation route reach up to 1% of atomic density [61]. The S-vacancies degrade electronic performance [64], resulting in a quenching of the luminescence and a hampering of the mobility of charge carriers [64]. Yet, in the meantime there are ways to repair the defects, e.g., using thiol-chemistry [15, 62, 64, 65]. The thiol-MoS_2 linkage can also be employed to covalently incorporate functional moieties into the 2D material [15, 66, 67]. In summary, the direct band gap of MoS_2 renders it a perfect fit for flexible optoelectronics and more [17, 19, 36]. The question arises, how can we prepare these outstanding materials in their 2D form? An overview of this question will be given in the chapter below before focusing on metal-mediated exfoliations.

3 2D material preparation concepts

The major challenge in 2D material preparation is the balance between material quality and production scalability. Two main routes can be identified [16, 23, 24], top-down processes (exfoliation) start with a parent-crystal and aim to separate the layered structures into the respective monolayers (while conserving material quality). Whereas, bottom-up processes rely on the controlled deposition of a single-layer, usually starting in part with gaseous precursors, a well-known example being chemical vapour deposition (CVD) [11, 16]. Each method has its own strengths and drawbacks (Fig. 4), for instance, CVD yields large-area monolayers, but their quality usually lacks compared to exfoliated samples, hiding the route to large-area high-quality materials via CVD behind a wall of optimization. Yet, once optimized the

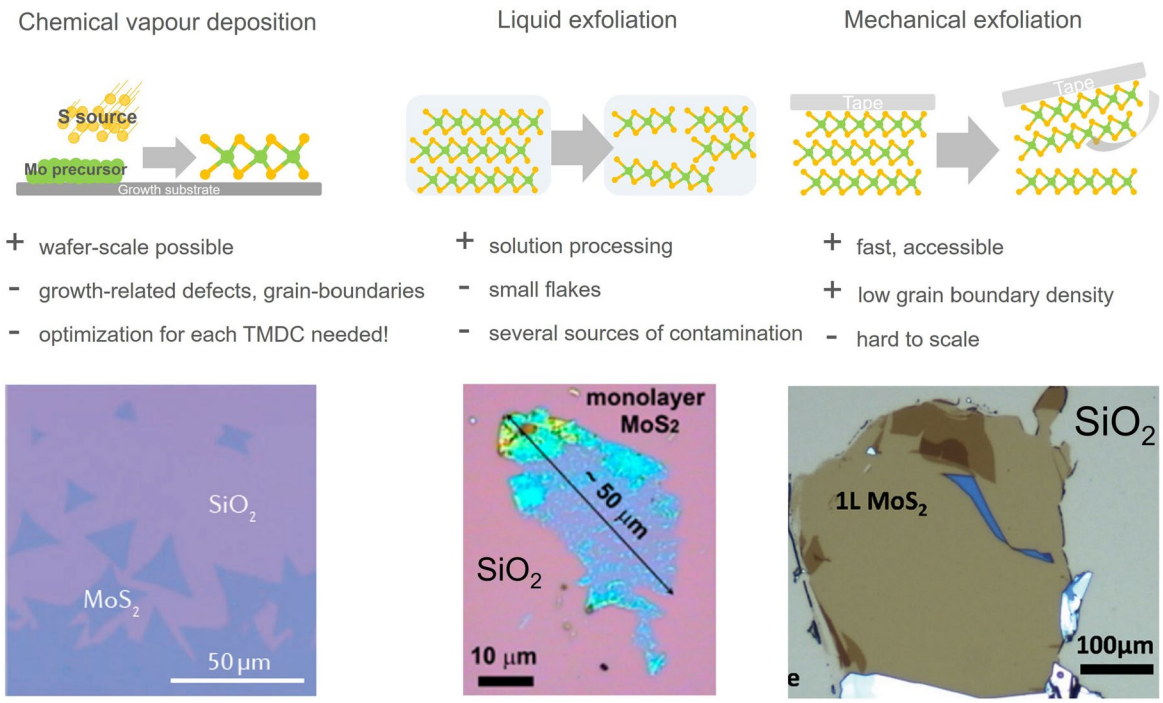

Fig. 4 Synthesis of 2D TMDCs with top-down and bottom-up approaches including pro and contra arguments for each method and examples for obtained MoS_2 monolayers. The optical micrograph of the CVD process (bottom left) shows the typical triangular-shaped grains and their merging into a continuous layer. This merging step can also cause defects like grain boundaries [68]. The liquid exfoliated flake (bottom middle) shows discontinuous single-layer areas. The mechanically exfoliated flakes, as exemplary shown in the bottom right micrograph for a gold-mediated exfoliation [38], can reach several hundreds of microns as detailed in the sections below. Some multilayers are apparent, yet the single-layer areas outweigh the multilayer areas. Bottom left, figure reprinted with permission from [72]. Copyright 2014 American Chemical Society. Bottom center, figure reprinted with permission from [71]. Copyright 2014 American Chemical Society. Bottom right, figure reprinted with permission from [38], copyright 2016 WILEY–VCH Verlag GmbH & Co. KGaA, Weinheim

CVD process is very powerful and capable of high-quality materials with very high scalability. There are several optimization parameters [27, 28] that need fine tuning to avoid defects or grain boundaries [68] and to finally reach single crystalline high-quality continuous films as summarized in previous reviews on this topic [27, 28]. In contrast, mechanical exfoliation is significantly less complex and readily produces high-quality 2D materials once a high-quality 3D crystal is available, thereby outsourcing the optimization to the supplier of the 3D crystal. On a side note, since the first (single) layer is usually the most challenging to grow in CVD-like techniques, it can be advantageous to grow large-area multilayers which can then be fed back into an exfoliation process to isolate several single layers with high-quality [49] as discussed in more detail in the application Sect. 4.3.

Liquid exfoliations (Fig. 4) are readily processable and resulting TMDC dispersions allow for printing applications [25, 69, 70], yet the method is limited by the small size, low quality, and contaminations of resulting monolayers [71].

On the other hand, mechanical exfoliation generally provides high-quality materials (ideally limited by parent crystal quality) and is mainly impeded by its low yield [2]. Flakes usually do not exceed tens to hundreds of microns, prohibiting large-scale processing (e.g., microcircuits [73]) and some common characterization methods relying on macroscopic samples. Despite the small scale, mechanical exfoliation has been a key enabler for lab-scale studies. The high quality and ease of access provided by this technique allowed for the study of several different 2D materials, where their high quality enabled the observation of quantum transport properties [29, 30]. In general, mechanical exfoliation has its roots in the scotch-tape technique. Here, the scotch tape provided the adhesion to physically thin down the layers until the monolayer is reached. Ultimately, the goal is to transition from a layered crystal to a monolayer. A simple modification improves mechanical exfoliation, the introduction of an exfoliation substrate. The scotch-tape exfoliation on ordinary substrates (e.g., silicon wafers) does not provide sufficient interaction, rendering the cleaving event for ending up with a single layer on the substrate rare. The competing vdW forces between layer in the crystal and the outermost layer with the exfoliation substrate are critical for successful exfoliation of the outermost layer with large-area and high yield [45]. Hence, ways of enhancing the substrate-crystal interactions are crucial and a good starting point are large, and uniform contact areas, maximizing the overall vdW interactions. For instance, studies showed improved exfoliation of graphene for oxygen-plasma-treated silicon wafers [37]. This method benefited from enhanced vdW interfaces via reduced contaminants and less trapped gaseous contaminants (decreasing vdW interaction via larger graphene-substrate distance). However, an exfoliation substrate capable of strong vdW interactions is needed. This is where gold and other noble metals came into play [32, 46]. Due to the high-quality promised by mechanical exfoliation, an accessible yet robust exfoliation process for TDMCs is highly desirable and finally enabled by gold-mediated exfoliations. The basic principles of these gold-mediated exfoliations are detailed in the following section.

3.1 Mechanism of Gold-mediated exfoliation and why other metals work too

The basic idea of metal-mediated exfoliations entails that the probability of cleaving the parent crystal such that the bottom-most layer remains as a monolayer on the metal surface is enhanced via TMDC-metal-specific interactions. The crystal intralayer vdW interactions must be overcome at the TMDCs-Metal interface to separate the outermost layer. Gold has proven quite successful in exfoliating layered materials beyond TMDCs as detailed in Sect. 4.2 [32, 38, 42–45]. For TMDCs, conceptually, the chalcogen-terminated layers provide a great opportunity for strong Au-Chalcogen interactions, since gold is well-known for its affinity towards chalcogen-based compounds (e.g., sulfur-containing thiols form self-assembled monolayers on gold) [74, 75]. But more generally, gold with its highly polarizable character favors dispersive (vdW) interactions [44, 45] and these interactions, are usually weak and non-directional. However, given a highly polarizable electron density, as it is the case for noble metals, the dispersive interactions reach intermediate strength (yet not as strong as a covalent bond) and are termed Covalent-like-quasi-bonding (CLQB) [44, 76]. Besides the strength compared to vdW interactions, the CLQB interactions are also more directional, i.e., involving wavefunction hybridizations [44, 76]. These interaction energies can reach beyond 0.5 eV per unit cell [44] and are therefore promising to overcome the intralayer vdW interactions in layered materials (e.g., interlayer binding for MoS_2 is ca. -0.34 eV [45]). For simplicity, this text will refer to dispersive interactions at the metal interfaces with vdW interactions, although in some cases CLQB might be more fitting.

An important question regarding the nature of the TMDC-Au interface arises—are Au–S bonds involved (potentially degrading material quality) or is it essentially a 2D-3D vdW heterostructure [10]. The answer depends on the history of the TMDC-Au interface since the conditions during the interface formation will render different interaction pathways viable [77]. For instance, one could evaporate gold onto MoS_2, leading to hot gold atoms bombarding the MoS_2 interface, introducing damages, defects, and chemical bonds (Fig. 5a, right) [77]. On the other hand, conformal contact between an Au film and MoS_2 via a mechanical transfer leads to an interface governed by vdW interactions (Fig. 5a, left) [77]. The challenge of forming damage-free Metal-TMDC interfaces also carries over into the domains

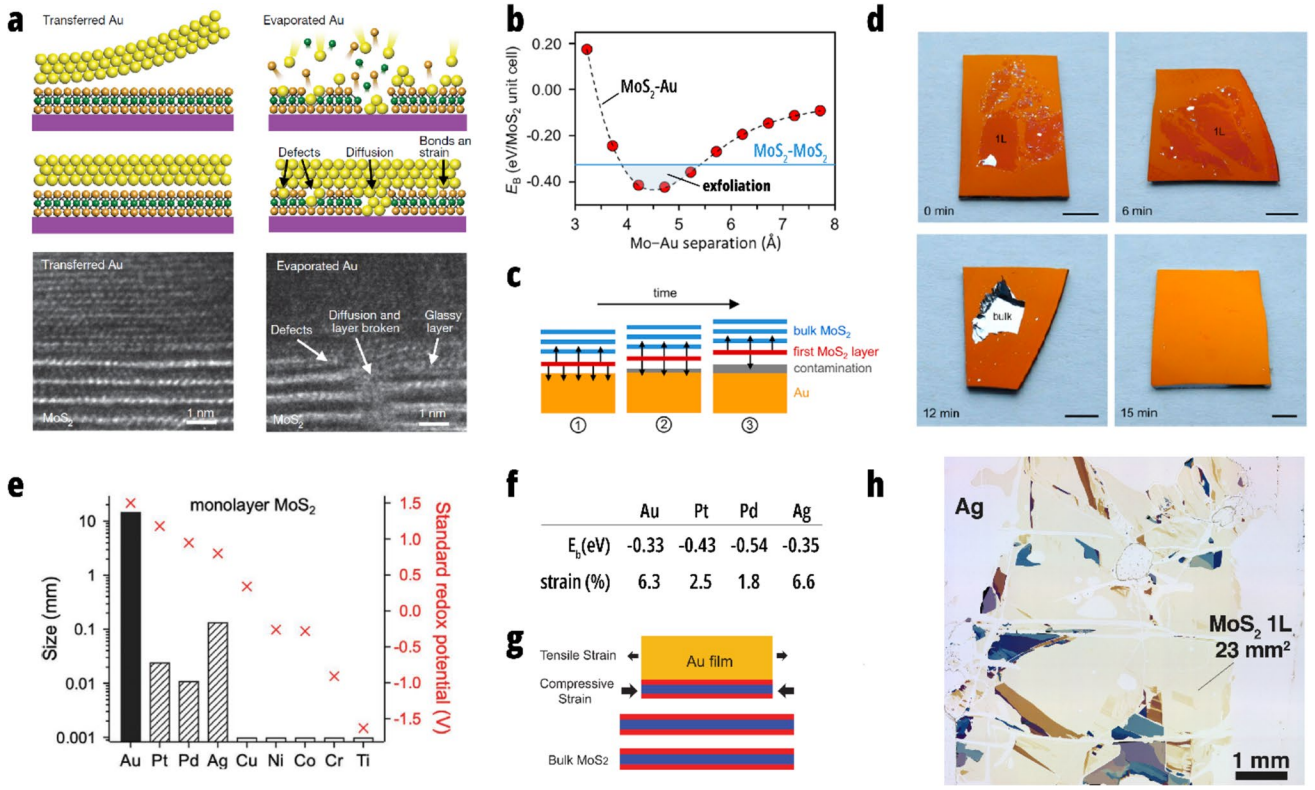

Fig. 5 Insights into the mechanism of metal-mediated exfoliations. **a** Two different principles of forming the Au-MoS_2 interface are detailed [77]. Transferred Au (left), a smooth and clean Au surface is brought into conformal contact with MoS_2. Evaporated Au (right) relies on direct deposition of (high-energy) Au on MoS_2, leading to different interaction pathways, also evident in the defects and damages in the TEM cross-section image below. **b** The vdW interaction mediated exfoliation via overcoming the (blue) interlayer MoS_2 binding energy is depicted (curve from vdW DFT calculations) [45]. The strict dependence on the MoS_2-Au separations suggests a smooth and clean gold surface is key to unlock this exfoliating vdW interaction regime, as depicted in (**c**). Here, even the build-up of a molecular contamination layer over time (e.g., air-borne carbohydrates from oil pumps running in the lab) can hinder the exfoliation [45], which degraded the exfoliation performance within minutes (**d**). Scale bars in **d** correspond to 5 mm. **e** The exfoliated single layer size for other metals than Au is shown [46]. A decrease in nobility (indicated via standard redox potential) is apparent. **f** Computed Metal-MoS_2 binding energies (optb88b-vdW-DF) [83] and compressive strain values applied to the metals to match the lattice constant of MoS_2 [81]. **g** Mechanism of strain-mediated exfoliation via disruption of the layer stacking registry at the metal-TMDC interface [84]. **h** Optical micrograph showing silver-mediated MoS_2 exfoliation performing on par with gold via a low-temperature (150 °C) annealing [47]. **a** Reprinted by permission from Springer Nature: Nature [77], copyright 2018. (**b–d**) Adapted with permission from [45]. Copyright 2018 American Chemical Society. **e** Reprinted with permission from [46]. Copyright 2020 The Authors. Advanced Materials Interfaces published by Wiley–VCH GmbH. **f** Top: Adapted with permission from [83]. Copyright 2016 by the American Physical Society. Bottom: Adapted with permission from [81]. Copyright 2014 American Chemical Society. **g** Reprinted with permission from [84]. Copyright 2018 by the American Physical Society. **h** Reprinted with permission from [47]. Copyright 2022 The Authors. Advanced Materials Interfaces published by Wiley–VCH GmbH

of contact engineering [77–79], where metal evaporation can induce damages leading to degraded performance and less control [80, 81]. This highlights the importance of damage-free purely vdW interfaces for both, exfoliations, and electrical contacts. Coming back to exfoliations, Velický et al., showed the pronounced vdW character present at the Au-MoS_2 interface formed via mechanical contact with ultra-clean and smooth gold surfaces [45]. The resulting Au–S distance in such a system (3.5 Å) [45] was found to be significantly larger than the typical covalent Au–S one (~ 2.2 Å) [45], excluding any Au–S bonds. Also therein, the process stability regarding contamination and roughness of the gold surface have been studied. Prolonged times in ambient air before applying the mechanical contact between the gold surface and the TMDC crystal led to dramatically less successful exfoliations [45]. This finding was rationalized by the buildup of airborne contaminations on gold [45, 82], disrupting the dispersive interactions. Gold surfaces are known to build up contaminations from thiols and airborne carbon contaminations (e.g., oil pumps running close by). Even a single molecular layer of contaminations on gold can disrupt the process since the critical Au–S distance to ensure exfoliation is sensitive to changes on the 1 Å level (Fig. 5b). The latter point also explains the reduced performance for

rougher gold surfaces. In summary, both above points are critical due to the steep distance dependence of these dispersive interactions (Fig. 5b), where even a slight increase in Mo-Au distance due to contamination will render the process a failure (Fig. 5c), as shown in Fig. 5d [45].

However, if one is to follow a pure binding energy argument, then other noble metals should at least perform on par with gold since the Metal-MoS_2 binding energy for gold is not the highest among the noble metals (Fig. 5f) [46, 48, 81, 83]. In reality, gold outperforms other noble metals easily as seen in Fig. 5e [46]. Here the standard redox potential is a guide to the metal's nobility. It is apparent that with decreasing nobility, the exfoliation performance decreases significantly. This shows that gold's interface is uniquely resistant against contamination and oxidation, which keeps the surface clear for strong vdW interactions, whereas less noble metals are plagued by oxide and more rapid contamination build up [46]. However, silver breaks the trend by outperforming Pt and Pd, hinting at an additional important factor: interfacial strain [46]. The strain due to lattice mismatch between the TMDC and the metal (Fig. 5f) might boost exfoliation performance [38, 46, 84] by disrupting layer registry in the parent crystal, preferring slip at the interfacing layer [84], leading to mostly single layer exfoliation (Fig. 5g). This would explain why silver outperforms Pd and Pt, which are the stronger candidates binding energy-wise (Fig. 5f). In that sense, gold further qualifies as ideal exfoliation candidate due to the large lattice mismatch providing strain [81]. In contrast to silver, gold strains the interfacing TMDC layer more homogenously, due to the lack of oxidation at the interface [46].

However, recently Johnston et al. [48], reported sizeable exfoliation (~ 125 µm for Pd) for different metals. Here, Palladium is especially interesting since the expected strain is low [48, 81] but the binding energy high [83], which would reinforce the notion that the latter is key. In contrast to the study by Velický et al. [46], the metals have been evaporated directly onto MoS_2 to avoid oxidation of the metal surface. Yet, this might cause additional defects, etc. as showcased in Fig. 5a [77], which potentially changes the exfoliation performance. Overall, the exact role of binding energy versus strain needs further studies, especially with more experimental strain values [46], since there is still a dramatic gap in reported exfoliation size for Pd vs. Au [46, 48, 85].

Finally, one degree of freedom is left to discuss: temperature. Some exfoliations were found to perform only after an annealing step around 150 °C–200 °C [43, 47]. This was attributed to contamination evaporation and or reconstruction of the metal-TMDC interface. Interestingly, this simple annealing step also allowed silver-mediated exfoliation with resulting single layers on par with gold (Fig. 5h) [47]. This might be explained by the relaxation of the otherwise stringent metal-TMDC interface condition via thermally activated surface reconstructions or contamination evaporation.

In summary, even aside from the details of the Au-TMDC interface formation [77] discussed earlier, the modus operandi for gold-mediated exfoliations is complicated. Two factors seem to play a critical role: the binding energy between layered material and metal [44, 48] and the interfacial strain due to lattice mismatch between these two [38, 46, 84]. The former is needed to overcome the interlayer binding energy in the bulk crystal and the latter facilitates high monolayer yield by disrupting the layer stacking registry in the bulk crystal [84]. In any case, a smooth and clean interface remains key. Noble metals provide both high polarizability to overcome the interlayer binding and in some cases the strain to facilitate exfoliation. Gold has a unique position among the noble metals, providing very high oxidation and contamination resistance [46], while also the ductile character enables easier conformal contact with the parent crystal.

3.2 State-of-the-art gold-mediated exfoliations: an overview

Gold-mediated exfoliations proved quite some capabilities (Table 1), in terms of monolayer size [42–45] and applicability to a variety of layered materials in general [44]. The compared exfoliated areas must be taken with a grain of salt, since most reported gold-mediated exfoliations reached the crystal limit. Meaning that only the parent crystal areas will limit the resulting single-layer areas [43]. Therefore, without referencing the starting crystal areas, it is difficult to compare exfoliated areas. Overall, it is clear that the strong dispersive interactions of gold are not exclusive to chalcogen-terminated materials (TMDCs) [44]. The most notable difference among the techniques is the way the gold is used as an exfoliation substrate—resulting in different possible mechanisms, as already discussed above. To illustrate the difference, one process scheme for each exfoliation route is given in Fig. 6. For instance, Desai et al. [38] evaporated gold directly onto the crystal. Whereas the work of Magda et al. [32] relied on template-stripped substrates, cleaved from mica. Template-stripping is perfectly suited for clean and ultra-flat gold surfaces on demand [86] and will be discussed in more depth in the guide Sect. 5.1. Some studies also investigated transfer methods away from gold onto insulating substrates, e.g., Desai et al. [38] directly transferred the Au-MoS_2 stack onto a silicon wafer using thermal-release tape (TRT), a subsequent KI/I_2 etch of Au revealed MoS_2 monolayers on silicon without etchant induced damages, thereby allowing polymer-free transfer. This etching step was subsequently included in many exfoliation procedures [42–44, 47]. The strong Au-TMDC interactions necessitate this etching step since it is not trivial to remove the exfoliated layers without it. However, a transfer is key since

Table 1 Survey of state-of-the-art gold-mediated exfoliations of several TMDCs and beyond

Au substrate	materials	MoS_2 1L exfoliated [mm^2]	MoS_2 1L transferred [mm^2]
Evaporation onto TMDC [38]	MoS_2 WS_2 WSe_2	~1.6×10^{-3}	~1.6×10^{-3}
Evaporated thin film [45]	MoS_2 $MoSe_2$ $MoTe_2$ WS_2 WSe_2 WTe_2 GaSe	~40	None
Evaporated thin film [44]	40 + (beyond TMDCs)	~25	~25
Template-strip mica [32]	MoS_2 WSe_2 Bi_2Te_3	~2.0×10^{-3}	~1.5×10^{-4}
Template-strip Si-wafer [42]	MoS_2 WS_2 $MoSe_2$ WSe_2 ReS_2	~50	~50
Template-strip Si-wafer [43]	MoS_2	~82	~82

Compared are the implementation of gold as an exfoliation substrate, the exfoliated TMDCs and the largest MoS_2 monolayer area reported. It is important to note that this is just an incomplete selection of gold-mediated exfoliations and is not exhaustive. Reprinted with permission from [43]. Copyright 2020 The Authors. Published by Wiley–VCH GmbH

the full potential of most 2D materials cannot be realized on gold. To accommodate for the importance of this transfer step, a separate guide Sect. (5.2) is dedicated to one such process. Before that, extensions and applications of gold-mediated exfoliations are reviewed below.

3.3 Extensions and applications of gold-mediated exfoliations

The previous section established how well gold-mediated exfoliations perform for the isolation of millimeter-scale 2D materials. However, this simple process still has many opportunities for extensions and improvements. For instance, even mono-elemental materials like black phosphorus (BP, Fig. 7 a) along with other non-chalcogen materials have been exfoliated with gold [44]. This solidifies the notion that gold provides strong dispersive interactions for many different vdW materials, commonly susceptible to these very interactions. A similar process was also extended to graphene and hBN using different metal films as stressors to enable layer-engineered large-area exfoliation of these materials [50]. The main limit for most gold-mediated single layers is the starting crystals. To tackle this, wafer-scale multi-layered 2D materials have been grown and then exfoliated using a layer-resolved splitting process via a controlled crack propagation with Nickel [49]. This resulted in wafer scale single layers up to 5 cm in scale and thereby addressed the crystal limit in an elegant manner. More generally, with large 2D materials unlocked, millimeter-scale single-layer devices [87] and ultimately integrated electronics [73] are within reach. Furthermore, crystals have been disassembled into large-scale single layers and then stacked again in a given order to create artificial lattices (Fig. 7b) [42]. In this way, millimeter-scale vdW heterostructures can be created [42, 44] which paved the way for the LEGO-like combination of many different materials, as envisioned before [6]. This vision entails the creation of artificial 3D vdW-stacked lattices composed of different 2D single-layer building blocks ("LEGO stones"), where gold-mediated exfoliations provide these large-scale single-layer building blocks for this endeavor. With the interlayer twist angle as another degree of freedom, one can also envision scaled-up twist-tronics [33, 34, 88, 89] and 2D quantum devices on the macroscopic scale [90]. Instead of chasing ultra-large continuous areas and then etching these into suitable geometries, it has been proven viable to directly perform patterned exfoliation (Fig. 7c) [39–41]. This way transistor channels can be directly realized without exposing the channel TMDC to polymeric photoresist. Usually, the as-exfoliated layers need to be transferred off the gold film to allow for meaningful device fabrication and non-quenched PL. However, using extremely thin and thereby electrically discontinuous gold films (e.g., 1.5 nm Au/ 0.5 nm Ti), it was possible to build field-effect transistors and observe PL with as-exfoliated single-layer MoS_2 on gold [44]. The intact PL on gold would otherwise require partly freestanding single layers. On this note, freestanding 2D materials are well sought after because they allow for substrate-free characterization of intrinsic properties. Since most exfoliation processes involve a polymer-based transfer to realize this suspended structure via a single layer on a hole-covered substrate, the quality of the suspended layer is already limited by the polymer residues. However, the direct exfoliation of free-standing 2D layers via gold films on hole-covered substrates has been demonstrated (Fig. 7d) [44]. This suspended layer is inherently polymer-free and reached up to 90% freestanding coverage [44], allowing a more unclouded view on the intrinsic properties of the exfoliated material. Yet, polymers are not the only residue source. The wet etching step of gold might also introduce

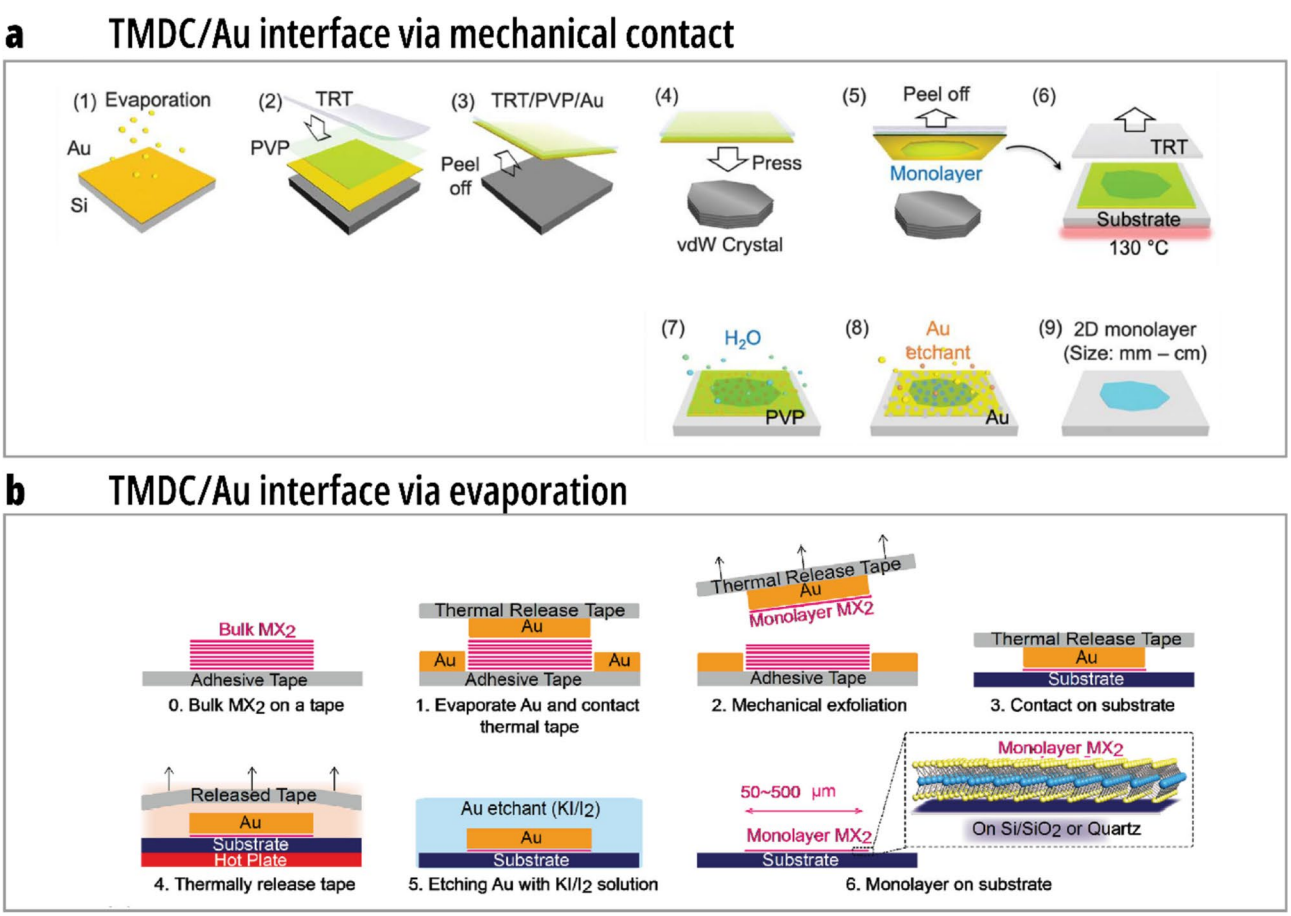

Fig. 6 Schematics of typical exfoliation processes from literature, both relying on a gold etching step. **a** TMDC-Au interface formed via mechanical contact [42] and **b** via Au evaporation [38]. It is noted that thermal release tape (TRT) is widely used in exfoliation processes, as well as KI/I_2 as gold etchant. **a** From [42]. Reprinted with permission from AAAS. **b** Reprinted with permission from [38], copyright 2016 WILEY–VCH Verlag GmbH & Co. KGaA, Weinheim

disorder and contamination. The strong TMDC-Au interactions which normally necessitate the etching step have been side stepped by employing a mesh structure. (Fig. 7d) [39]. In this gold mesh, the freestanding parts of the 2D material can be transferred onto a target substrate without the need to etch gold, simply via a mechanical lift-off at the gold edges. Using this method, vdW heterostructures have been prepared in an array-like fashion [39].

Several devices have been realized using these gold-mediated exfoliations, most prominently field effect transistors [38, 39, 41, 44, 49]. It was also shown that the previously reported super-acid treatment can boost the quantum yield of gold-exfoliated MoS_2 [38]. As mentioned before, for a very thin electrically discontinuous gold layer it was possible to exfoliate and subsequently build field-effect transistors on the as-exfoliated flakes on gold without the need to transfer onto an insulating substrate [44]. Overall, the gold-mediated exfoliations discussed here provide the building blocks ready to be integrated into the device structures previously discussed. For more insights into these 2D device concepts, the reader is referred to previous reviews [10, 14, 19, 54, 78].

Finally, to provide some more insights into an established exfoliation workflow, a walkthrough of a gold-mediated exfoliation and transfer [43] is provided.

3.4 Guide towards exfoliation substrates—ultrasmooth template-stripped gold

The template-stripping procedure describes an experimentally simple replica process, able to transfer the flatness of a given template (mica, polished silicon wafers) to the target film (metal films, oxide films, polymers) over large areas [86, 91]. This method is especially appealing due to its simplicity yet being able to replicate topographic features in the angstrom dimensions over large areas. Traditionally deposited gold films (e.g., physical vapour deposition, PVD), typically grow under the formation of islands, leading to a high roughness for these films [86, 92]. Yet, smooth surfaces are crucial and the use of ultra-flat templates to yield smooth

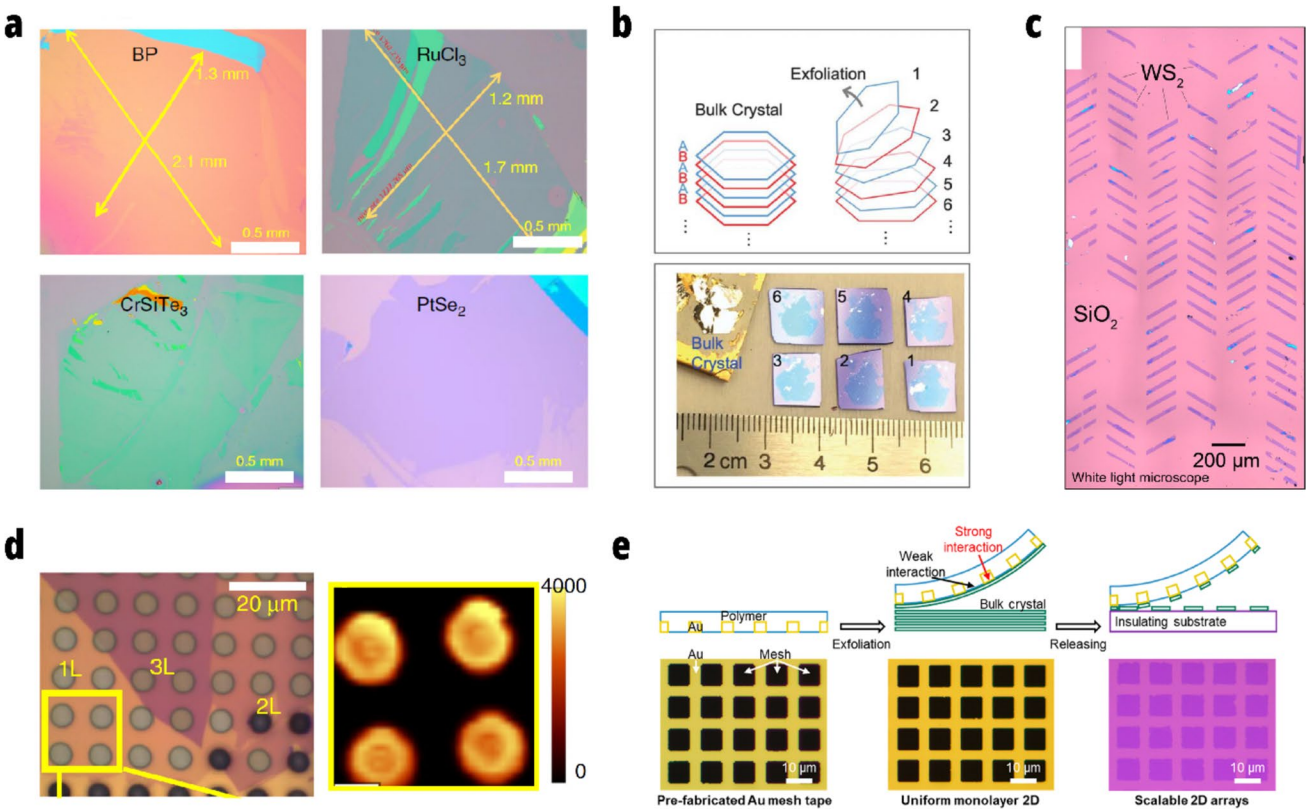

Fig. 7 Extensions of gold-mediated exfoliations. **a** Extending the range of exfoliated materials, including monoelemental black phosphorus (BP) [44]. It is apparent that the process is not limited to chalcogen-containing materials. **b** Disassembling 2D crystals into single layers before reassembling these in large-scale artificial lattices [42]. **c** Patterned exfoliation of WS_2 by etching the gold-TMDC structure before transfer [41]. **d** Exfoliation of freestanding layers via gold films on hole-covered substrates [44]. A PL intensity map is shown on the right, with quenched PL on gold and emission from the suspended structures. **e** Etch-free and dry exfoliation and transfer via gold-mesh structures [39]. The freestanding parts of the exfoliated area can be transferred onto the target substrate without etching gold. The non-suspended layers remain on gold. **a**, **d** Reprinted by permission from Springer Nature: Nature Communications [44], copyright 2020. **b** From [42]. Reprinted with permission from AAAS. **c** Reprinted with permission from [41]. Copyright 2019 American Chemical Society. **e** Reprinted with permission from [39]. Copyright 2021 American Chemical Society

metal films is therefore highly desirable. In the context of gold-mediated TMDC exfoliations, the capability to produce smooth and clean gold surfaces in a robust and simple manner renders template-stripping the perfect route towards gold-based exfoliation substrates. Magda et al. [32] proved the capabilities of a template-strip-based exfoliation early on, using mica as template. However, due to micas layered nature, it is prone to template residues [86]. Thus, silicon wafers are a very attractive template candidate, known for their low roughness over very large areas. Template-stripping of gold via polished silicon wafer templates is illustrated in Fig. 8.

The polished silicon wafer acts as ultra-flat template, a thin gold film is deposited and subsequently an adhesion layer (epoxy glue) is added to attach solid support (glass slide). The resulting sandwich can be cleaved at the point of weakest adhesion, i.e., the wafer-gold interface, releasing the fresh and ultra-smooth gold interface. The roughness of the template is replicated by the gold interface, revealing extremely smooth gold surfaces over large areas [86, 92]. Furthermore, the smooth gold surface is protected from environmental contaminations, due to being hidden at the wafer-gold interface. This allows for the preparation of ultra-smooth and fresh gold interfaces on demand. Thus, mitigating a well-known issue of metal surface contaminations via oxygen, thiols and airborne hydrocarbons (which is critical for the needed intimate contact between metal and layered material as explained in Sect. 4.1) [85, 86]. Ultimately, template-stripping is not limited to the preparation of smooth metals, but rather provides a general route towards smooth films cleaved off a template [86]. Thus, rendering it a very valuable tool in the context of 2D materials and vdW assemblies, which heavily rely on flat interfaces [56, 93]. As we will show below template-stripping is the perfect route for exfoliation substrates for gold-mediated TMDCs exfoliation.

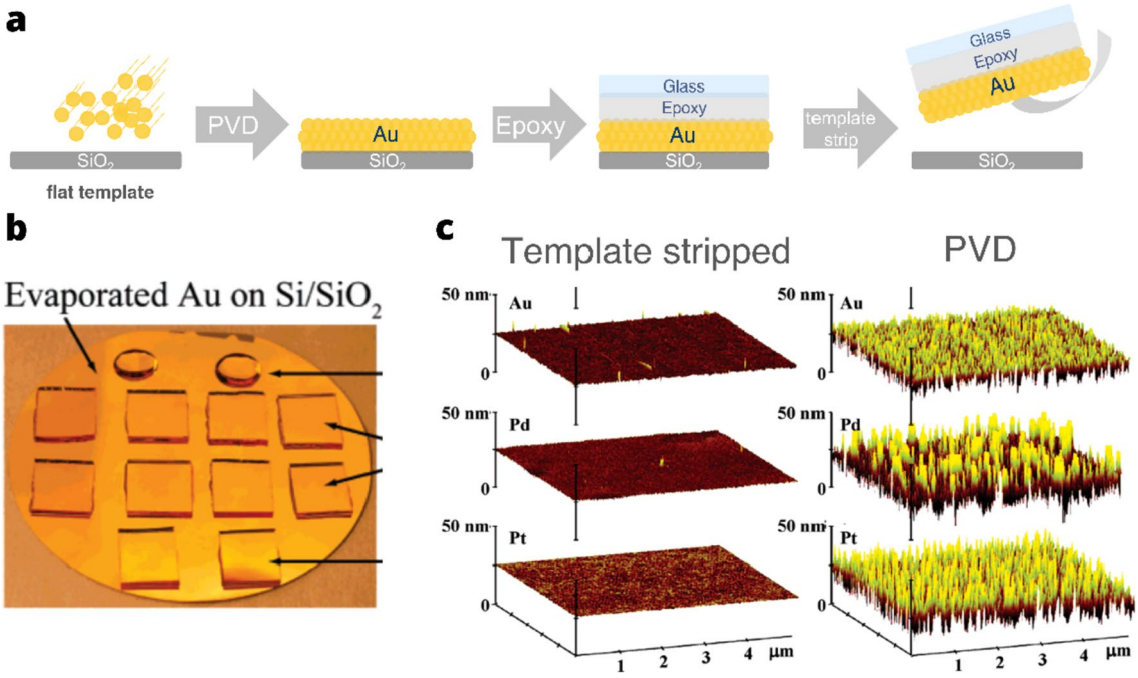

Fig. 8 Template-stripping for ultra-smooth metal surfaces on demand. **a** Schematic of template-stripped Au film fabrication. **b** Gold-coated silicon wafer depicting several glass chips glued onto the gold film, ready for template stripping [92]. The smooth metal surface is protected until needed, thereby enabling smooth & clean surfaces on demand. **c** AFM study to reveal the much smoother template-stripped metal surfaces compared to the as-deposited ones (PVD) [92]. **b**, **c** Reprinted with permission from [92]. Copyright 2007 American Chemical Society

3.5 Mechanical exfoliation with template-stripped gold—a ready-to use recipe

The exfoliation process starts with the stripping of both the parent crystal and gold, to access fresh interfaces of both. Combining MoS_2 and template-stripped Au along with a mild annealing leads to ultra-large area exfoliation of MoS_2 on gold as depicted in Fig. 9. At this point, a sacrificial copper layer (~ 600 nm) below the Au layer (~ 200 nm) has been introduced for the transfer, as described later. To recap the recipe; it is crucial to start with a smooth parent crystal, ideally freshly cleaved MoS_2 supported by heat-resistant tape (Kapton). The MoS_2 is paired with a freshly template-stripped gold substrate and finger pressure ensures conformal contact. Baking the Kapton-MoS_2-Au sandwich at 200 °C for 1 min on a hotplate leads to the exfoliation of MoS_2 monolayers, uncovered by stripping off the parent MoS_2 on the Kapton tape after a short cooldown (~ 2 min). The Kapton-tape should cover the MoS_2 well to support it over its whole dimensions while avoiding large overcuts to minimize tape residues on gold. This exfoliation results in a robust and accessible route for millimeter-scale TMDC monolayers [43]. To address the crystal-limited character of the process, a monolayer yield based on the initial crystal area in contact with Au (Fig. 9b) is determined, resulting in circa 68% monolayer yield. The monolayer yield (Fig. 9b right) is clearly impeded by multilayers present in the exfoliated areas. However, the exfoliation of multilayers, to some extent, should also depend on the quality of the parent crystal interface, where ripples and defects favor multilayer generation (e.g., due to tear-in processes at these defects) [43]. It is important to note that it might be fruitful to link crystal features to exfoliation results, as done in Fig. 9b. Some studies vaguely note the crystal limit of their exfoliation. However, if possible, the monolayer yield should be defined with respect to their initial crystal dimensions. Additionally, parent crystal features (e.g., ripples and wrinkles) deteriorate exfoliation results, as previously shown [43]. Henceforth, to push the (crystal-) limit of exfoliations, routes for smoother and larger crystals are key.

3.6 Polymer-free Au-based transfer—a ready-to-use recipe

Cu can be etched orthogonally to Au, leaving the Au-MoS_2 foil floating on the Cu etch solution [43]. This way, Au can be used for exfoliation as well as transfer. This way a polymer-free transfer route is presented. $FeCl_3$ etches Cu quickly without damage to MoS_2 observable [43]. The transfer process is depicted in Fig. 10. XPS studies of MoS_2 on SiO_2 confirmed the complete etching of Au and Cu [43]. The transfer process starts with exfoliated 1L MoS_2 on Au and is

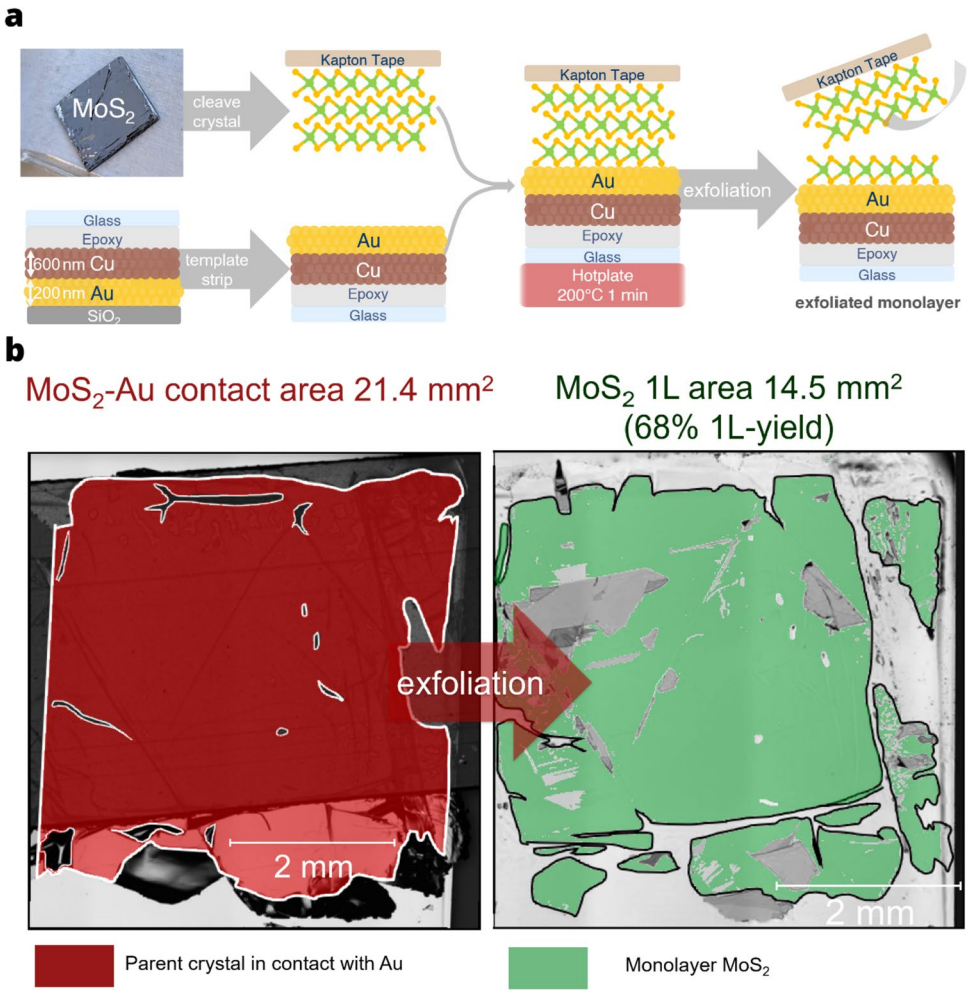

Fig. 9 **a** The exfoliation process. The template strip reveals a fresh gold surface, which is combined with a freshly cleaved bulk crystal of MoS_2. After applying a quick annealing step, the cooled-down stack is cleaved by removing the tape with bulk MoS_2, revealing exfoliated MoS_2 on gold. **b** Estimation of exfoliation area. The monolayer yield, as a fraction of parent crystal area in contact with Au, is approximately 68% and mainly impeded by the wrinkles of the parent crystal and multilayer generation. The largest continuous single layer shows an area of 14.5 mm^2

capable of deterministically transferring the latter onto SiO_2 (Fig. 10b). The MoS_2 1L area on Au (11 mm^2) is conserved, as well as the relative positions of the MoS_2 features. Further atomic force microscopy characterization of the transferred single layer proves the wrinkle-free transfer and the expected step height [11, 22, 43, 94, 95] (Fig. 10c). Optical characterizations show the typical PL emission for single-layer MoS_2 [9, 21] and the characteristic Raman shifts [96–98], a statement of the monolayer's integrity after transfer and etching. This enables to isolate single layers on arbitrary substrates where the quality of the bulk crystal is conserved, which side steps the difficult optimization processes needed to grow a continuous single layer in bottom-up processes. This defines the enabling essence of exfoliations, where once a starting crystal is (commercially) available, high-quality monolayers can be isolated, opening a whole palette of 2D materials to be targeted. The term high quality used here thereby refers to the limit set by the starting crystal. This renders the quality essentially limited by the supplier, a topic that needs to be studied in more detail in the future. The results render this process a promising route for polymer-free transfer, incorporated into an easy-to-use state-of-the-art exfoliation process. These high-quality 2D materials might be key to further unravel substrate influence on electronic and other properties in large areas [99]. Furthermore, no organic solvent is involved in the transfer, which potentially allows for polymer-free assembly of complex vdW heterostructures tuned with organic interlayers [100].

4 Conclusion and outlook

This review presents recent developments in gold-mediated exfoliations beyond scotch tape accompanied by a methods walkthrough for such a process. To date, gold-mediated exfoliations allow robust and accessible isolation of millimeter-scale single layers, mainly limited in size by the starting crystals. A plethora of different layered materials have been exfoliated, proving that these gold-mediated interactions are not exclusive to chalcogen-terminated TMDCs. Over time, many extensions to metal-mediated exfoliations have been made, e.g., patterned exfoliations and direct exfoliations of

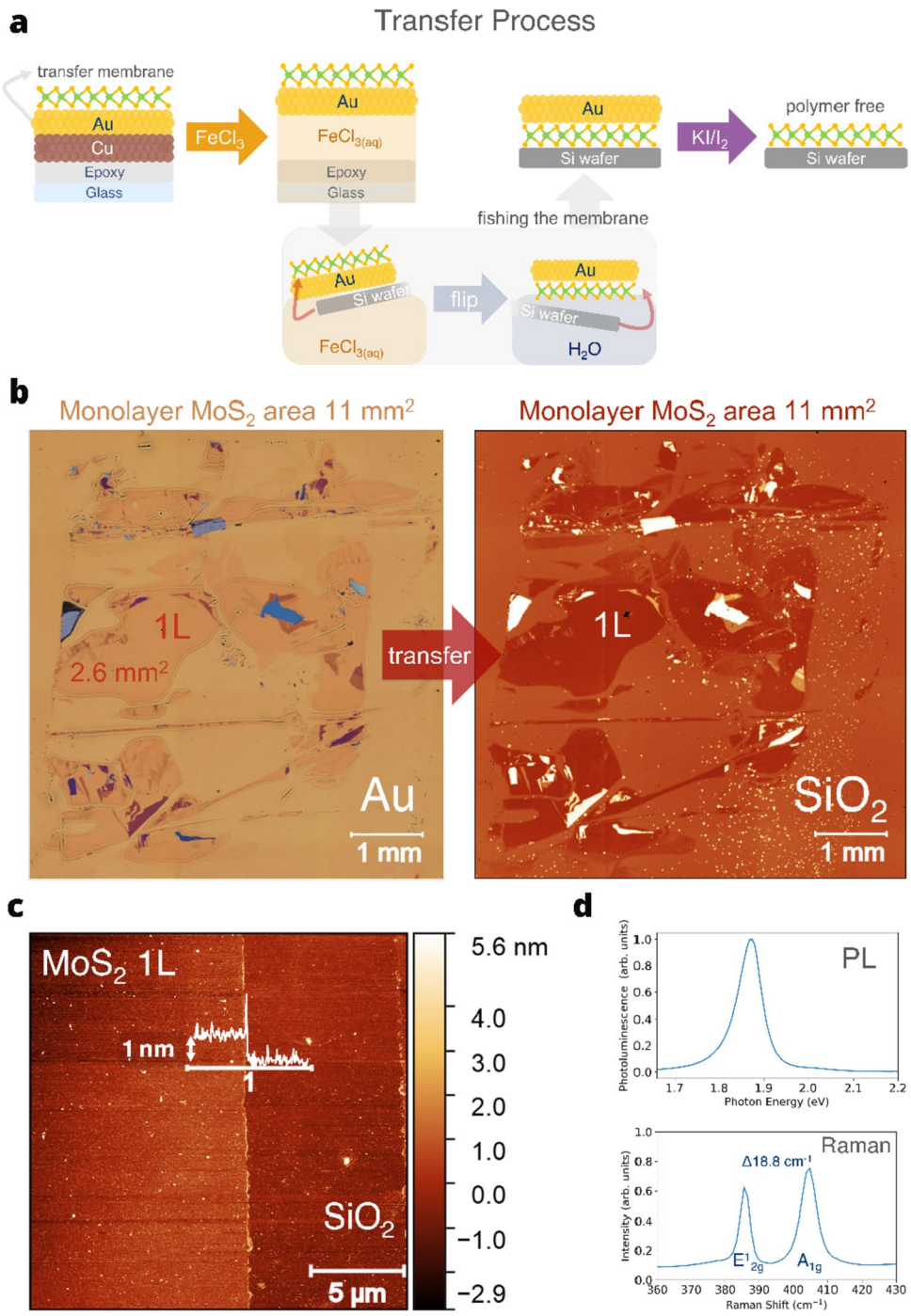

Fig. 10 Au-based transfer [43] (following Au-based exfoliation) exploiting orthogonal etching of Cu and Au. The Cu-etchant $FeCl_3$ does not attack MoS_2. The floating Au-MoS_2 foil is scooped with a wafer piece and transferred onto H_2O for washing off etchant residues. The foil is flipped and floated on clean H_2O, the target substrate (silicon wafer) is used to fish the foil, MoS_2 facing the substrate. Finally, the foil is dried to ensure conformal contact of MoS_2 and the target, supported by additional annealing (80 °C for 1 h). The transfer is finished by etching the Au with KI/I_2. **b** Deterministic transfer of MoS_2 on Au (left, 1L regions masked red) onto a silicon wafer (right, red channel image). The MoS_2 features and relative positions remain unchanged. The process deterministically transfers the whole MoS_2 area. **c** MoS_2 1L step height on silicon wafer measured with AFM. No ripples or wrinkles are present, proving the smooth transfer capabilities. **d** PL and Raman measurements (532 nm excitation Laser). **c**, **d** Adapted with permission from [43]. Copyright 2020 The Authors. Published by Wiley–VCH GmbH

freestanding single layers. However, the modus operandi of metal-mediated exfoliations is not clear yet. The two main factors are the large binding energy between 2D materials and (clean and oxide-free) noble metals, which allows to overcome interlayer binding. While the second factor is interfacial strain, favoring a slip of the interfacing layer, facilitating the high single-layer yield observed experimentally. The balance between binding energies and strain needs to be studied in more depth. It is clear, however, that gold is in a unique position due to its high resistance to oxidation and surface contamination, which allows to employ the high binding energies and strain uniformly.

These matured gold-mediated exfoliations unlocked 2D building blocks on the millimeter scale, which renders the previously envisioned [6] stacking of 2D building blocks into artificial 3D layered crystals more relevant than ever. This exfoliated palette of 2D building blocks might enable the assembly of macroscopic van der Waals heterostructures,

or twisttronics in the near future. In addition, with more and more (organic) layered single crystals available, these metal-mediated exfoliations might provide a feasible route to reach the unexplored two-dimensional limit of newly emerging materials [101, 102]. Finally, mechanical exfoliation, plagued by its low yield and poor scalability, was never considered as an industry solution for 2D materials. Yet, since the described methods are mainly limited by parent crystal dimensions, a change of mind might be fruitful, focusing on large-scale high-quality parent crystals for even larger exfoliated areas, pushing towards up-scalable processes in a practical fashion (e.g., roll-to-roll).

Acknowledgements The authors gratefully acknowledge proofreading by Sarah Grützmacher and Daniel Steffen Rühl. The authors gratefully acknowledge the financial support of DFG (Project number 182087777—SFB 951). This work was carried out in the framework of the Joint Lab GEN_FAB and was supported by the HySPRINT Innovation Lab at Helmholtz Zentrum Berlin.

Funding Open Access funding enabled and organized by Projekt DEAL.

Data availability The data for the non-reprinted plots of this review are available from the corresponding author upon reasonable request.

Declarations

Conflict of interest The authors have no competing interests to declare that are relevant to the content of this article.

References

1. K.S. Novoselov, A.K. Geim, S.V. Morozov, D. Jiang, Y. Zhang, S.V. Dubonos, I.V. Grigorieva, A.A. Firsov, Science **306**, 666 (2004)
2. K.S. Novoselov, D. Jiang, F. Schedin, T.J. Booth, V.V. Khotkevich, S.V. Morozov, A.K. Geim, Proc Natl Acad Sci USA **102**, 10451 (2005)
3. P. Joensen, R.F. Frindt, S.R. Morrison, Mater Res Bull **21**, 457 (1986)
4. A.K. Geim, K.S. Novoselov, Nat Mater **6**, 183 (2007)
5. M.J. Allen, V.C. Tung, R.B. Kaner, Chem Rev **110**, 132 (2010)
6. A.K. Geim, I.V. Grigorieva, Nature **499**, 419 (2013)
7. A. H. Castro Neto, F. Guinea, N. M. R. Peres, K. S. Novoselov and A. K. Geim, Rev Mod Phys **81**, 109 (2009).
8. K.F. Mak, J. Shan, Nat Photonics **10**, 216 (2016)
9. K.F. Mak, C. Lee, J. Hone, J. Shan, T.F. Heinz, Phys Rev Lett **105**, 2 (2010)
10. D. Jariwala, T.J. Marks, M.C. Hersam, Nat Mater **16**, 170 (2017)
11. M. Chhowalla, H.S. Shin, G. Eda, L.J. Li, K.P. Loh, H. Zhang, Nat Chem **5**, 263 (2013)
12. G. Wang, A. Chernikov, M. M. Glazov, T. F. Heinz, X. Marie, T. Amand, and B. Urbaszek, Rev Mod Phys **90**, (2018).
13. J. R. Schaibley, H. Yu, G. Clark, P. Rivera, J. S. Ross, K. L. Seyler, W. Yao, and X. Xu, Nat Rev Mater **1**, (2016).
14. R. Frisenda, A.J. Molina-Mendoza, T. Mueller, A. Castellanos-Gomez, H.S.J. van der Zant, Chem Soc Rev **47**, 3339 (2018)
15. S. Bertolazzi, M. Gobbi, Y. Zhao, C. Backes, P. Samorì, Chem Soc Rev **47**, 6845 (2018)
16. S. Manzeli, D. Ovchinnikov, D. Pasquier, O. v. Yazyev, and A. Kis, Nat Rev Mater **2**, (2017).
17. Q.H. Wang, K. Kalantar-Zadeh, A. Kis, J.N. Coleman, M.S. Strano, Nat Nanotechnol **7**, 699 (2012)
18. M. Velický, P.S. Toth, Appl Mater Today **8**, 68 (2017)
19. M. Chhowalla, D. Jena, H. Zhang, Nat Rev Mater **1**, 1 (2016)
20. Z. Hu, Z. Wu, C. Han, J. He, Z. Ni, W. Chen, Chem Soc Rev **47**, 3100 (2018)
21. A. Splendiani, L. Sun, Y. Zhang, T. Li, J. Kim, C.-Y. Chim, G. Galli, F. Wang, Nano Lett **10**, 1271 (2010)
22. B. Radisavljevic, A. Radenovic, J. Brivio, V. Giacometti, A. Kis, Nat Nanotechnol **6**, 147 (2011)
23. H. Li, J. K. Huang, Y. Shi, and L. J. Li, Adv Mater Interfaces **6**, (2019).
24. C. Song, G. Noh, T.S. Kim, M. Kang, H. Song, A. Ham, M.K. Jo, S. Cho, H.J. Chai, S.R. Cho, K. Cho, J. Park, S. Song, I. Song, S. Bang, J.Y. Kwak, K. Kang, ACS Nano **14**, 16266 (2020)
25. V. Nicolosi, M. Chhowalla, M.G. Kanatzidis, M.S. Strano, J.N. Coleman, Science **340**, 72 (2013)
26. J.N. Coleman, M. Lotya, A. O'Neill, S.D. Bergin, P.J. King, U. Khan, K. Young, A. Gaucher, S. De, R.J. Smith, I.V. Shvets, S.K. Arora, G. Stanton, H.Y. Kim, K. Lee, G.T. Kim, G.S. Duesberg, T. Hallam, J.J. Boland, J.J. Wang, J.F. Donegan, J.C. Grunlan, G. Moriarty, A. Shmeliov, R.J. Nicholls, J.M. Perkins, E.M. Grieveson, K. Theuwissen, D.W. McComb, P.D. Nellist, V. Nicolosi, Science **331**, 568 (2011)
27. L. Sun, G. Yuan, L. Gao, J. Yang, M. Chhowalla, M.H. Gharahcheshmeh, K.K. Gleason, Y.S. Choi, B.H. Hong, Z. Liu, Nat Rev Methods Primers **1**, 5 (2021)
28. Z. Cai, B. Liu, X. Zou, H.-M. Cheng, Chem Rev **118**, 6091 (2018)
29. Y. Zhang, Y.-W. Tan, H.L. Stormer, P. Kim, Nature **438**, 201 (2005)
30. X. Cui, G.-H. Lee, Y.D. Kim, G. Arefe, P.Y. Huang, C.-H. Lee, D.A. Chenet, X. Zhang, L. Wang, F. Ye, F. Pizzocchero, B.S. Jessen, K. Watanabe, T. Taniguchi, D.A. Muller, T. Low, P. Kim, J. Hone, Nat Nanotechnol **10**, 534 (2015)
31. T. Roy, M. Tosun, J.S. Kang, A.B. Sachid, S.B. Desai, M. Hettick, C.C. Hu, A. Javey, ACS Nano **8**, 6259 (2014)
32. G.Z. Magda, J. Petõ, G. Dobrik, C. Hwang, L.P. Biró, L. Tapasztó, Sci Rep **5**, 3 (2015)
33. Y. Cao, V. Fatemi, S. Fang, K. Watanabe, T. Taniguchi, E. Kaxiras, P. Jarillo-Herrero, Nature **556**, 43 (2018)
34. Y. Cao, V. Fatemi, A. Demir, S. Fang, S.L. Tomarken, J.Y. Luo, J.D. Sanchez-Yamagishi, K. Watanabe, T. Taniguchi, E. Kaxiras, R.C. Ashoori, P. Jarillo-Herrero, Nature **556**, 80 (2018)
35. https://commons.wikimedia.org/wiki/File:Nobelpriset_i_fysik_2010.png (accessed 31.10.2022).
36. D. Lembke, S. Bertolazzi, A. Kis, Acc Chem Res **48**, 100 (2015)
37. Y. Huang, E. Sutter, N.N. Shi, J. Zheng, T. Yang, D. Englund, H.J. Gao, P. Sutter, ACS Nano **9**, 10612 (2015)

38. S.B. Desai, S.R. Madhvapathy, M. Amani, D. Kiriya, M. Hettick, M. Tosun, Y. Zhou, M. Dubey, J.W. Ager, D. Chrzan, A. Javey, Adv Mater **28**, 4053 (2016)
39. Z. Li, L. Ren, S. Wang, X. Huang, Q. Li, Z. Lu, S. Ding, H. Deng, P. Chen, J. Lin, Y. Hu, L. Liao, Y. Liu, ACS Nano **15**, 13839 (2021)
40. V. Nguyen, H. Gramling, C. Towle, W. Li, D.H. Lien, H. Kim, D.C. Chrzan, A. Javey, K. Xu, J. Ager, H. Taylor, J Micro Nanomanuf (2019). https://doi.org/10.1115/1.4045259
41. H.M. Gramling, C.M. Towle, S.B. Desai, H. Sun, E.C. Lewis, V.D. Nguyen, J.W. Ager, D. Chrzan, E.M. Yeatman, A. Javey, H. Taylor, ACS Appl Electron Mater **1**, 407 (2019)
42. L. Fang, W. Wenjing, B. Yusong, C.S. Hoon, L. Qiuyang, W. Jue, H. James, Science **367**, 903 (2020)
43. M. Heyl, D. Burmeister, T. Schultz, S. Pallasch, G. Ligorio, N. Koch, E.J.W. List-Kratochvil, Phys Status Solidi Rapid Res Lett **14**, 2000408 (2020)
44. Y. Huang, Y. H. Pan, R. Yang, L. H. Bao, L. Meng, H. L. Luo, Y. Q. Cai, G. D. Liu, W. J. Zhao, Z. Zhou, L. M. Wu, Z. L. Zhu, M. Huang, L. W. Liu, L. Liu, P. Cheng, K. H. Wu, S. B. Tian, C. Z. Gu, Y. G. Shi, Y. F. Guo, Z. G. Cheng, J. P. Hu, L. Zhao, G. H. Yang, E. Sutter, P. Sutter, Y. L. Wang, W. Ji, X. J. Zhou, and H. J. Gao, Nat Commun **11**, (2020).
45. M. Velický, G.E. Donnelly, W.R. Hendren, S. McFarland, D. Scullion, W.J.I. Debenedetti, G.C. Correa, Y. Han, A.J. Wain, M.A. Hines, D.A. Muller, K.S. Novoselov, H.D. Abruna, R.M. Bowman, E.J.G. Santos, F. Huang, ACS Nano **12**, 10463 (2018)
46. M. Velický, G.E. Donnelly, W.R. Hendren, W.J.I. DeBenedetti, M.A. Hines, K.S. Novoselov, H.D. Abruña, F. Huang, O. Frank, Adv Mater Interfaces **7**, 2001324 (2020)
47. M. Heyl, S. Grützmacher, S. Rühl, G. Ligorio, N. Koch, and E. J. W. List-Kratochvil, Adv Mater Interfaces **9**, (2022).
48. A. C. Johnston and S. I. Khondaker, Adv Mater Interfaces **9**, (2022).
49. J. Shim, S.H. Bae, W. Kong, D. Lee, K. Qiao, D. Nezich, Y.J. Park, R. Zhao, S. Sundaram, X. Li, H. Yeon, C. Choi, H. Kum, R. Yue, G. Zhou, Y. Ou, K. Lee, J. Moodera, X. Zhao, J.H. Ahn, C. Hinkle, A. Ougazzaden, J. Kim, Science **362**, 665 (2018)
50. J.-Y. Moon, M. Kim, S.-I. Kim, S. Xu, J.-H. Choi, D. Whang, K. Watanabe, T. Taniguchi, D. Seop Park, J. Seo, S. Ho Cho, S.-K. Son, and J.-H. Lee, Sci Adv **6**, (2020)
51. Y.C. Lin, C.C. Lu, C.H. Yeh, C. Jin, K. Suenaga, P.W. Chiu, Nano Lett **12**, 414 (2012)
52. W.S. Leong, H. Wang, J. Yeo, F.J. Martin-Martinez, A. Zubair, P.C. Shen, Y. Mao, T. Palacios, M.J. Buehler, J.Y. Hong, J. Kong, Nat Commun **10**, 1 (2019)
53. K. S. Novoselov, A. Mishchenko, A. Carvalho, and A. H. Castro Neto, Science **353**, (2016).
54. Y. Liu, N. O. Weiss, X. Duan, H. C. Cheng, Y. Huang, and X. Duan, Nat Rev Mater **1**, (2016).
55. R. Frisenda, E. Navarro-Moratalla, P. Gant, D. Pérez De Lara, P. Jarillo-Herrero, R.V. Gorbachev, A. Castellanos-Gomez, Chem Soc Rev **47**, 53 (2018)
56. D. Rhodes, S.H. Chae, R. Ribeiro-Palau, J. Hone, Nat Mater **18**, 541 (2019)
57. L. Wang, I. Meric, P.Y. Huang, Q. Gao, Y. Gao, H. Tran, T. Taniguchi, K. Watanabe, L.M. Campos, D.A. Muller, J. Guo, P. Kim, J. Hone, K.L. Shepard, C.R. Dean, Science **342**, 614 (2013)
58. E. Gibney, Nature **522**, 274 (2015)
59. S. Park, N. Mutz, T. Schultz, S. Blumstengel, A. Han, A. Aljarb, L.-J. Li, E.J.W. List-Kratochvil, P. Amsalem, N. Koch, Mater **5**, 025003 (2018)
60. W. Zhou, X. Zou, S. Najmaei, Z. Liu, Y. Shi, J. Kong, J. Lou, P.M. Ajayan, B.I. Yakobson, J.C. Idrobo, Nano Lett **13**, 2615 (2013)
61. J. Hong, Z. Hu, M. Probert, K. Li, D. Lv, X. Yang, L. Gu, N. Mao, Q. Feng, L. Xie, J. Zhang, D. Wu, Z. Zhang, C. Jin, W. Ji, X. Zhang, J. Yuan, Z. Zhang, Nat Commun **6**, 1 (2015)
62. Z. Yu, Y. Pan, Y. Shen, Z. Wang, Z.Y. Ong, T. Xu, R. Xin, L. Pan, B. Wang, L. Sun, J. Wang, G. Zhang, Y.W. Zhang, Y. Shi, X. Wang, Nat Commun **5**, 1 (2014)
63. H. Qiu, T. Xu, Z. Wang, W. Ren, H. Nan, Z. Ni, Q. Chen, S. Yuan, F. Miao, F. Song, G. Long, Y. Shi, L. Sun, J. Wang, X. Wang, Nat Commun **4**, 1 (2013)
64. S. Bertolazzi, S. Bonacchi, G. Nan, A. Pershin, D. Beljonne, P. Samorì, Adv Mater **29**, 1606760 (2017)
65. M. Makarova, Y. Okawa, M. Aono, J Phys Chem C **116**, 22411 (2012)
66. S. Dalgleish, L. Reissig, Y. Shuku, G. Ligorio, K. Awaga, E.J.W. List-Kratochvil, Sci Rep **9**, 1 (2019)
67. D.M. Sim, M. Kim, S. Yim, M.J. Choi, J. Choi, S. Yoo, Y.S. Jung, ACS Nano **9**, 12115 (2015)
68. X. Xu, T. Schultz, Z. Qin, N. Severin, B. Haas, S. Shen, J.N. Kirchhof, A. Opitz, C.T. Koch, K. Bolotin, J.P. Rabe, G. Eda, N. Koch, Adv Mater **30**, 1803748 (2018)
69. E. Varrla, C. Backes, K.R. Paton, A. Harvey, Z. Gholamvand, J. McCauley, J.N. Coleman, Chem Mater **27**, 1129 (2015)
70. K.R. Paton, E. Varrla, C. Backes, R.J. Smith, U. Khan, A. O'Neill, C. Boland, M. Lotya, O.M. Istrate, P. King, T. Higgins, S. Barwich, P. May, P. Puczkarski, I. Ahmed, M. Moebius, H. Pettersson, E. Long, J. Coelho, S.E. O'Brien, E.K. McGuire, B.M. Sanchez, G.S. Duesberg, N. McEvoy, T.J. Pennycook, C. Downing, A. Crossley, V. Nicolosi, J.N. Coleman, Nat Mater **13**, 624 (2014)
71. N. Liu, P. Kim, J.H. Kim, J.H. Ye, S. Kim, C.J. Lee, ACS Nano **8**, 6902 (2014)
72. H. Schmidt, S. Wang, L. Chu, M. Toh, R. Kumar, W. Zhao, A. H. Castro Neto, J. Martin, S. Adam, B. Özyilmaz, and G. Eda, Nano Lett **14**, 1909 (2014).
73. S. Wachter, D.K. Polyushkin, O. Bethge, T. Mueller, Nat Commun **8**, 1 (2017)
74. J.P. Folkers, P.E. Laibinis, G.M. Whitesides, Langmuir **8**, 1330 (1992)
75. J.C. Love, L.A. Estroff, J.K. Kriebel, R.G. Nuzzo, G.M. Whitesides, Chem Rev **105**, 1103 (2005)
76. Z.X. Hu, X. Kong, J. Qiao, B. Normand, W. Ji, Nanoscale **8**, 2740 (2016)
77. Y. Liu, J. Guo, E. Zhu, L. Liao, S. Lee, M. Ding, I. Shakir, V. Gambin, Y. Huang, and X. Duan, Nature (2018).
78. A. Allain, J. Kang, K. Banerjee, A. Kis, Nat Mater **14**, 1195 (2015)
79. Y. Wang, J.C. Kim, R.J. Wu, J. Martinez, X. Song, J. Yang, F. Zhao, A. Mkhoyan, H.Y. Jeong, M. Chhowalla, Nature **568**, 70 (2019)
80. Y. Guo, D. Liu, and J. Robertson, Appl Phys Lett **106**, (2015).
81. C. Gong, L. Colombo, R.M. Wallace, K. Cho, Nano Lett **14**, 1714 (2014)
82. T. Smith, J Colloid Interface Sci **75**, 51 (1980)
83. M. Farmanbar and G. Brocks, Phys Rev B **93**, (2016).
84. H. Sun, E. W. Sirott, J. Mastandrea, H. M. Gramling, Y. Zhou, M. Poschmann, H. K. Taylor, J. W. Ager, and D. C. Chrzan, Phys Rev Mater **2**, (2018).
85. M. Velický, G.E. Donnelly, W.R. Hendren, S. McFarland, D. Scullion, W.J.I. DeBenedetti, G.C. Correa, Y. Han, A.J. Wain, M.A. Hines, D.A. Muller, K.S. Novoselov, H.D. Abruña, R.M. Bowman, E.J.G. Santos, F. Huang, ACS Nano **12**, 10463 (2018)
86. N. Vogel, J. Zieleniecki, I. Köper, Nanoscale **4**, 3820 (2012)
87. S. Rühl, M. Heyl, F. Gärisch, S. Blumstengel, G. Ligorio, E.J.W. List-Kratochvil, Phys Status Solidi **15**, 2100147 (2021)

88. D.M. Kennes, M. Claassen, L. Xian, A. Georges, A.J. Millis, J. Hone, C.R. Dean, D.N. Basov, A.N. Pasupathy, A. Rubio, Nat Phys **17**, 155 (2021)
89. C.N. Lau, M.W. Bockrath, K.F. Mak, F. Zhang, Nature **602**, 41 (2022)
90. X. Liu, M.C. Hersam, Nat Rev Mater **4**, 669 (2019)
91. N. Vogel, M. Jung, M. Retsch, W. Knoll, U. Jonas, I. Köper, Small **5**, 821 (2009)
92. E. A. Weiss, G. K. Kaufman, J. K. Kriebel, Z. Li, R. Schalek, and G. M. Whitesides, Langmuir 9686 (2007).
93. Y. Liu, Y. Huang, X. Duan, Nature **567**, 323 (2019)
94. A. Gurarslan, Y. Yu, L. Su, Y. Yu, F. Suarez, S. Yao, Y. Zhu, M. Ozturk, Y. Zhang, L. Cao, ACS Nano **8**, 11522 (2014)
95. G. Eda, H. Yamaguchi, D. Voiry, T. Fujita, M. Chen, M. Chhowalla, Nano Lett **11**, 5111 (2011)
96. C. Lee, H. Yan, L.E. Brus, T.F. Heinz, J. Hone, S. Ryu, ACS Nano **4**, 2695 (2010)
97. H. Li, Q. Zhang, C.C.R. Yap, B.K. Tay, T.H.T. Edwin, A. Olivier, D. Baillargeat, Adv Funct Mater **22**, 1385 (2012)
98. M. Timpel, G. Ligorio, A. Ghiami, L. Gavioli, E. Cavaliere, A. Chiappini, F. Rossi, L. Pasquali, F. Gärisch, E. J. W. List-Kratochvil, P. Nozar, A. Quaranta, R. Verucchi, and M. V. Nardi, NPJ 2D Mater Appl **5**, (2021).
99. S. Park, T. Schultz, D. Shin, N. Mutz, A. Aljarb, H.S. Kang, C.H. Lee, L.J. Li, X. Xu, V. Tung, E.J.W. List-Kratochvil, S. Blumstengel, P. Amsalem, N. Koch, ACS Nano **15**, 14794 (2021)
100. C. Hsu, C. Lin, J. Huang, C. Chu, K. Wei, and L. Li, ACS Nano 5031 (2012).
101. D. Burmeister, H. A. Tran, J. Müller, M. Guerrini, C. Cocchi, J. Plaickner, Z. Kochovski, E. J. W. List-Kratochvil, and M. J. Bojdys, Angewandte Chemie—International Edition **61**, (2022).
102. D. Burmeister, M.G. Trunk, M.J. Bojdys, Chem Soc Rev **50**, 11559 (2021)